J Biol Inorg Chem (2009) 14:1227–1241
DOI 10.1007/s00775-009-0566-9

ORIGINAL PAPER

Probing intermediates in the activation cycle of [NiFe] hydrogenase by infrared spectroscopy: the Ni-SI_r state and its light sensitivity

Maria-Eirini Pandelia · Hideaki Ogata · Leslie J. Currell · Marco Flores · Wolfgang Lubitz

Received: 27 March 2009 / Accepted: 26 June 2009 / Published online: 21 July 2009

Abstract The [NiFe] hydrogenase from the sulphate-reducing bacterium *Desulfovibrio vulgaris* Miyazaki F is reversibly inhibited in the presence of molecular oxygen. A key intermediate in the reactivation process, Ni-SI_r, provides the link between fully oxidized (Ni-A, Ni-B) and active (Ni-SI_a, Ni-C and Ni-R) forms of hydrogenase. In this work Ni-SI_r was found to be light-sensitive ($T \leq 110$ K), similar to the active Ni-C and the CO-inhibited states. Transition to the final photoproduct state (Ni-SL) was shown to involve an additional transient light-induced state (Ni-SI_{1961}). Rapid scan kinetic infrared measurements provided activation energies for the transition from Ni-SL to Ni-SI_r in protonated as well as in deuterated samples. The inhibitor CO was found not to react with the active site of the Ni-SL state. The wavelength dependence of the Ni-SI_r photoconversion was examined in the range between 410 and 680 nm. Light-induced effects were associated with a nickel-centred electronic transition, possibly involving a change in the spin state of nickel (Ni^{2+}). In addition, at $T \leq 40$ K the CN^- stretching vibrations of Ni-SL were found to be dependent on the colour of the monochromatic light used to irradiate the species, suggesting a change in the interaction of the hydrogen-bonding network of the surrounding amino acids. A possible mechanism for the photochemical process, involving displacement of the oxygen-based ligand, is discussed.

Keywords [NiFe] hydrogenase · *Desulfovibrio vulgaris* · Rapid scan Fourier transform infrared · Light sensitivity · Activation energies · Isotope effect · Wavelength dependence · Carbon monoxide

Electronic supplementary material The online version of this article (doi:10.1007/s00775-009-0566-9) contains supplementary material, which is available to authorized users.

M.-E. Pandelia · H. Ogata · L. J. Currell · M. Flores · W. Lubitz (✉)
Max-Planck-Institut für Bioanorganische Chemie,
Stiftstrasse 34-36,
45470 Mülheim an der Ruhr,
Germany
e-mail: lubitz@mpi-muelheim.mpg.de

Present Address:
M. Flores
Department of Chemistry and Biochemistry,
Arizona State University,
Tempe, AZ 85287-1604,
USA

Introduction

Hydrogenases are metalloenzymes found in the metabolic pathway of a wide variety of anaerobic and hydrogen-oxidizing microorganisms [1]. They catalyse the elementary reversible reaction

$$H_2 \rightleftharpoons 2H^+ + 2e^-.$$

Such enzymes couple either oxidation of dihydrogen or reduction of protons to H_2 to the activity of nearby redox centres. According to the metal content of their active site, they can be classified into three major categories: (1) [NiFe] hydrogenases, with nickel and iron forming a hetero-binuclear active centre [2–5], (2) [FeFe] hydrogenases, with a bimetallic iron centre linked to a [4Fe–4S] cubane forming the so-called H-cluster [6, 7] and (3) iron–sulphur cluster-free hydrogenases (Hmd) or [Fe] hydrogenases from methanogenic archaea consisting of a mononuclear iron [8].

The [NiFe] hydrogenase from the sulphate-reducing bacterium *Desulfovibrio vulgaris* Miyazaki F is a periplasmic membrane attached enzyme [9]. It has a molecular mass of 91 kDa and consists of two subunits. The heteronuclear Ni–Fe

centre is located at the heart of the large subunit; with two cysteinyl ligands linking the two metal ions (Fig. 1). Nickel is coordinated further by two other cysteinyl residues in a terminal fashion and has an open coordination site opposite to the bridging Cys549. This free coordination site is believed to serve as the contact position for dihydrogen during the catalytic process, as the enzyme cycles through the different redox states. In this process the nickel changes oxidation state, whereas the iron always remains in the divalent state (Fe^{2+}). The iron is bridged to nickel by the Cys84 and Cys549 residues (Fig. 1) and is further coordinated by strong σ- and π-ligands, i.e. two cyanides (CN^-) and one carbonyl (CO) [10], which stabilize the iron into a low oxidation and low-spin state (Fe^{2+}, $S = 0$). Each cyanide ligand is proposed to form up to two hydrogen bonds with the surrounding amino acids (e.g. Arg479, Pro478, Pro501, Ser502—*D. vulgaris* numbering), whereas the carbonyl is surrounded by more hydrophobic residues (e.g. Leu482, Val500). A third bridging ligand is often present (labelled as X in Fig. 1), whose identity and composition varies depending on the catalytic state of the enzyme [4, 5]. The small subunit contains one $[3Fe–4S]^{1+/0}$ cluster and two $[4Fe–4S]^{2+/1+}$ clusters [3, 11]. These clusters mediate the electron transfer between the active site and the redox partner of the hydrogenase (e.g. cytochrome c_3) [1].

The function of the [NiFe] hydrogenases can be inhibited in the presence of oxygen [12–14], carbon monoxide [15, 16] and other substances [17, 18]. Thus, aerobic isolation of the enzyme results in inactive states with oxygen-based ligands bound to the bimetallic site. The most oxidized states are called Ni-A and Ni-B (Fig. 2). They are both paramagnetic states ($S = 1/2$) related to a Ni^{3+} in the d_{z^2} ground state, but exhibit different spectroscopic properties [2] and activation

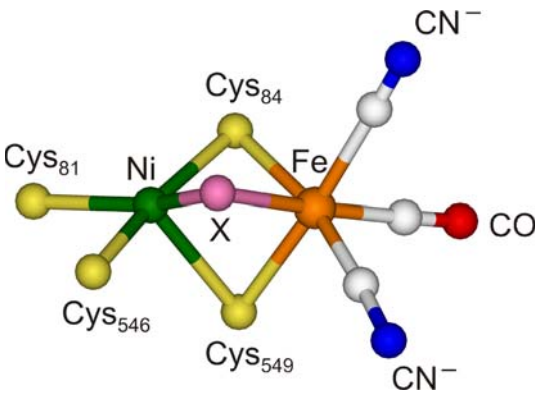

Fig. 1 Active site of the [NiFe] hydrogenase from *Desulfovibrio vulgaris* Miyazaki F in the oxidized forms. The elements are represented by the following colours: *orange* (iron), *green* (nickel), *yellow* (sulphur), *white* (carbon), *red* (oxygen) and *blue* (nitrogen). The third bridging ligand X is shown in *pink*. The numbering of the cysteine ligands from the protein is given

kinetics [12, 19]. Ni-B (ready) is quickly activated in the presence of H_2 or under reducing conditions, whereas Ni-A (unready) requires longer times [12] and is suggested not to interact directly with H_2 [16, 20]. It has been proposed that the differences between Ni-A and Ni-B are associated with the identity of the third ligand bridging nickel and iron (labelled as X in Fig. 1). For Ni-B the ligand was identified as OH^- [21], whereas for Ni-A it is suggested to be a di-oxo species (presumably OOH^-) as shown by X-ray crystallographic experiments [14, 22].

One-electron reduction of Ni-B produces the Ni-SI_r state (Ni_r-S/Ni-SI_I by other authors). This reaction is pH-dependent [23–25], showing that the transition from Ni-B to Ni-SI_r is coupled to proton transfer [23, 25]. Electron paramagnetic resonance (EPR) experiments have shown that Ni-SI_r is an EPR-silent[1] species (Ni^{2+}) [26, 27]. In addition, other spectroscopic data have shown the presence of a third bridging ligand that hinders the functional ability of Ni-SI_r [5, 24, 28, 29]. Thus, two different mechanisms have been proposed to explain the transition from Ni-B to Ni-SI_r. Some authors have suggested that the proton is directly transferred to OH^-, resulting in a water molecule as the third bridging ligand in Ni-SI_r [30, 31], which can then be easily removed under physiological conditions. Others have suggested that the proton is transferred to one of the coordinating cysteinyl residues that acts as a base, which facilitates the later protonation of OH^- to water [29]. The second mechanism considers that OH^- remains as the third bridging ligand in the active site of Ni-SI_r. In this scheme Ni-SI_r is in acid–base equilibrium with a transient state $(Ni\text{-}SI_r)_{II}$ (state in brackets in Fig. 2), which retains the H_2O ligand loosely bound to the active centre.

After removal of the H_2O ligand, the enzyme is able to enter the functional cycle. This cycle is comprised of three catalytically active states (Fig. 2), in which the redox components (active site and iron–sulphur centres) change their oxidation levels. Ni-SI_a is the most oxidized active state and is EPR-silent (Ni^{2+}). Further one-electron reduction of Ni-SI_a leads to the paramagnetic active state Ni-C (Ni^{3+}, $S = 1/2$), with the substrate bound to the Ni–Fe site. This was shown by electron–nuclear double resonance (ENDOR) and hyperfine sublevel correlation (HYSCORE) spectroscopies, first for the regulatory hydrogenase from *Ralstonia eutropha* [32] and later for the standard hydrogenase from *D. vulgaris* Miyazaki F [33], where a hydride (H^-) was identified as the third bridging

[1] Integer-spin ground states can be characterized as EPR-silent either if they are diamagnetic ($S = 0$) or if they cannot be observed with conventional microwave X/Q/W band frequencies (i.e. $S \geq 1$, where the zero-field splitting is larger than the microwave quantum). So far no experimental evidence exists from high-field EPR studies for the reduced hydrogenase states for whether they are associated with a high-spin or a low-spin state for Ni^{2+}.

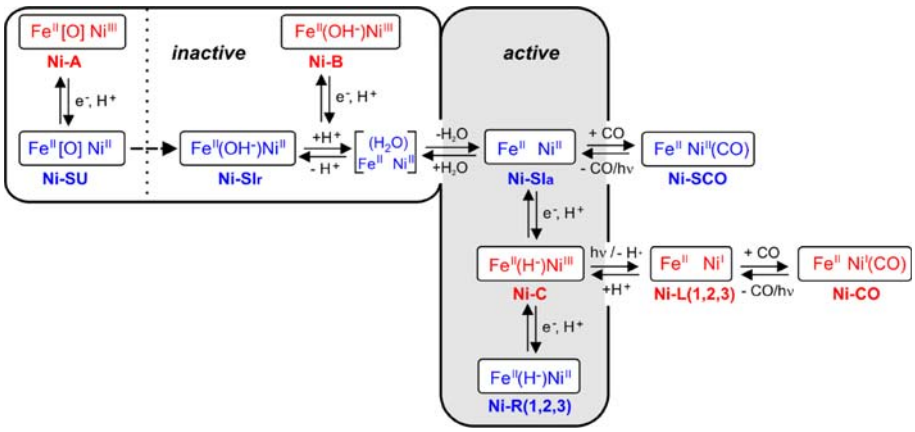

Fig. 2 Proposed activation and catalytic mechanism for the standard, oxygen-sensitive [NiFe] hydrogenases. The inhibition by CO and the light sensitivity of specific states are also depicted. The formal oxidation state of the nickel and iron ions are shown for each state along with the proposed inorganic bridging ligand X present in the active site. Note that for Ni-A and Ni-SU the exact identity of X is not yet known. *Red* denotes the electron paramagnetic resonance (EPR)-active states. The EPR-silent states are given in *blue*

ligand in Ni-C. At cryogenic temperatures ($T \leq 170$ K) the Ni-C state has been shown to be light-sensitive [34]. Illumination at such temperatures converts Ni-C into a new paramagnetic state denoted as Ni-L. This light-induced transition was shown by EPR spectroscopy to be associated with the loss of the hydride bridging ligand upon conversion to Ni-L. This reaction is fully reversible in the dark at higher temperatures ($T \geq 200$ K). Further reduction of Ni-C produces the Ni-R states, which are again EPR-silent. Up to three different Ni-R states have been observed by infrared spectroscopic studies [31]. For all divalent reduced states (Ni-SI, Ni-R) L-edge X-ray absorption spectroscopy (XAS) [35] and L-edge X-ray magnetic circular dichroism (XMCD) [36] studies are consistent with a high-spin nickel state. However, recent theoretical studies suggest a low-spin state for Ni^{2+} in the Ni-SI states [37].

Furthermore, [NiFe] hydrogenases can be inhibited by carbon monoxide. It has been shown that in the active enzyme, extrinsic CO binds terminally to nickel at the open coordination site [38]. An EPR-silent CO-inhibited state (Ni-SCO) [26, 39] is formed if CO binds to the Ni-SI_a state, whereas a paramagnetic CO-inhibited state (Ni-CO) results from binding of CO to the Ni-L state [40] (Fig. 2). Similar to the Ni-C state, Ni-SCO (EPR-silent, inactive) and Ni-CO (paramagnetic, inactive) are also light-sensitive at cryogenic temperatures. This effect can be directly correlated with structural changes in the active site upon illumination (i.e. dissociation of the extrinsic CO) [26]. However, up to the present there is little information on the light sensitivity of the states related to the oxygenic inhibition of the enzyme. This kind of property, if observed, can be used to characterize structural features of the active site in such states and thus provide insight into the reactivation process of the enzyme, in particular for the study of the inactive EPR-silent states (e.g. Ni-SI_r).

Since some of the states participating in the catalytic cycle of the enzyme [i.e. Ni-SI states, Ni-R (1, 2, 3) states] shown in Fig. 2 are EPR-silent [26, 27, 30], their structural and chemical properties cannot be studied by EPR spectroscopy. In such cases Fourier transform infrared (FTIR) spectroscopy has proved to be very valuable for following redox changes in the active site of hydrogenases, as the strong π- and σ-ligands (CO, CN^-) [26] are sensitive probes of electronic changes (i.e. electron density on iron, solvent interactions and intermolecular hydrogen bonding of the CN^- ligands with nearby proton-donor amino acids) [26]. Vibrational spectroscopy can thus provide an effective means to identify each redox state, to follow them in the reaction cycle and to reveal associated structural and electronic changes.

In this work we investigated the Ni-SI_r state and its light sensitivity using FTIR spectroscopy. Temperature-dependent back-conversion kinetics, study of the isotope effect (H/D) on the kinetic rates, wavelength dependence of the photoconversion and effect of carbon monoxide are reported. The light-induced effects are discussed and related to structural rearrangements in the active site of the *D. vulgaris* Miyazaki F hydrogenase.

Materials and methods

Sample preparation

Hydrogenase from the anaerobic bacterium *D. vulgaris* Miyazaki F was isolated from 50 L cultures as previously described [41]. The pH of the purified enzyme was kept at pH 7.4 in tris(hydroxymethyl)aminomethane(Tris)/HCl buffer solutions.

Samples in D_2O

The aerobically purified enzyme was 20-fold diluted and reconcentrated in D_2O (99.9%, Deutero) based tris(hydroxymethyl)aminomethane buffer with pD 7.4 (pD = pH + 0.41). This procedure was repeated five times. The sample was finally concentrated and fully reduced with D_2 gas (N27, Air Liquide). Reduction with D_2 was performed using a home-built gas mixer, in which the pressure was controlled with a manometer in a steel chamber of 30 cm^3. Oxidation of the sample was obtained by exposure to atmospheric air.

CO-inhibited enzyme

The aerobically purified hydrogenase was reduced with H_2 in the presence of methyl viologen ($E_m = -448$ mV, Aldrich) for 10 min. H_2 was flushed out of the solution, which was subsequently saturated with CO (N47, Air Liquide) for 15 min on ice. The sample was transferred to the FTIR cell under 100% CO atmosphere (glove bag) and immediately frozen in liquid N_2.

FTIR spectroscopy

Low temperature measurements (10 K $\leq T \leq$ 110 K) were carried out with a Bruker IFS 66v/S FTIR spectrometer with 2 cm^{-1} spectral resolution using an Oxford Instruments Optistat CF cryostat. The spectrometer is equipped with a mercury cadmium telluride (MCT) photoconductive detector. The temperature was controlled using an ITC 503 temperature controller (Oxford Instruments). Kinetic measurements were carried out in rapid scan mode. Samples were irradiated in situ for 5 min with a slide projector (250 W halogen lamp, 24 V) equipped with an electronic shutter (Compor). The temperature dependence of the measured kinetic rates was fitted with the Arrhenius equation [42]: $\ln k = \ln A - E_a/RT$, where k is the rate constant (s^{-1}), A is the frequency factor (s^{-1}), E_a is the activation energy (kJ mol^{-1}), R is the ideal gas constant (8.314472 J K^{-1} mol^{-1}) and T is the temperature (K). Illumination for various times at different wavelengths in the range between 410 and 680 nm was carried out with an OPO laser (OPOTEK Vibrant 355 II). A conversion of approximately 100% could be achieved at 40 K after 10 min of illumination. This temperature was chosen since complete conversion took place faster than at higher temperatures. The laser repetition rate was 10 Hz. The total energy of the excitation light was measured with a calibrated power meter. The excitation energy was chosen so that the number of photons was the same for all selected wavelengths and corresponded to the number of photons present with excitation light at 630 nm and 1.5 mJ $pulse^{-1}$ total energy. The excitation energy at an arbitrary wavelength λ can be calculated according to the equation

$$P(\lambda) = P(630) \times \frac{630}{\lambda}.$$

Samples of 15 μL were placed between sapphire windows (80-μm path length) and inserted in the cryostat at low temperatures. Measurements at room temperature were carried out in a 50 μL transmission cell equipped with calcium fluoride (CaF_2) windows with 1 cm^{-1} resolution. The temperature was regulated and kept at the desired value with the help of a thermostat (RML, LAUDA). In an FTIR spectrometer light from a low output power He–Ne laser ($\lambda = 633$ nm, red light) passes through the sample compartment and monitors the position of the moving mirror. In some cases an anti-reflection coated germanium filter was placed between the sample and the interferometer. This filter serves to shield the sample from the He–Ne laser and its transmission is greater than 80% between 5,000 and 500 cm^{-1}. Usually it is omitted so as to increase the sensitivity of the infrared measurements. Data were collected and baseline corrected using the OPUS software package (Bruker). Kinetic data fitting was performed using MATLAB 7.0.

EPR spectroscopy

EPR measurements were carried out with a Bruker ESP-300 continuous wave X-band spectrometer equipped with an Oxford Instruments helium flow cryostat and an ITC 503 temperature controller.

Results

Room temperature FTIR measurements

Figure 3a shows the FTIR spectrum of the aerobically isolated [NiFe] hydrogenase from *D. vulgaris* Miyazaki F at 297 K (24 °C). In this spectrum we identified the bands corresponding to the Ni-A, Ni-B and Ni-SI_r states. The vibrational frequencies corresponding to these states as well as of all the redox intermediate states present in *D. vulgaris* are summarized in Table 1. These values are similar to the ones reported previously for *D. vulgaris*, with the exception of those for the Ni-SU state [25], which has been now accurately resolved and for which the data are now in agreement with data reported for other known hydrogenases [31]. All other EPR-silent states which do not correspond to known redox intermediates will be denoted with their CO vibration frequencies as a subscript. The bands in the region from 2,000 to 1,900 cm^{-1} are associated with the CO vibrations of three different states

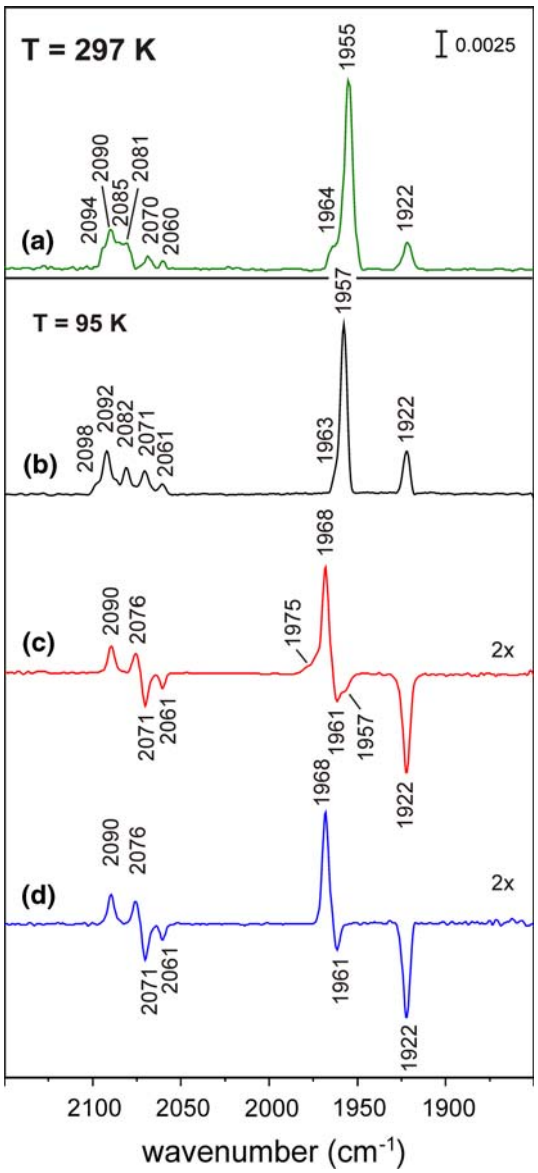

Fig. 3 Fourier transform infrared (FTIR) spectra of the aerobically isolated [NiFe] hydrogenase from *D. vulgaris* Miyazaki F, at 297 K (*a*) and 95 K (*b*). Light-minus-dark difference spectrum at 95 K (*c*) and after dark adaptation and reillumination (*d*). Ni-SI_r and Ni-SI_{1961} are the dark educts (negative bands), which upon illumination convert to the Ni-SL product state (positive bands). The vibrational frequencies for the CO and CN^- stretching vibrations are given on all spectra (see Table 1). The *y*-axis represents the infrared absorbance

(i.e. Ni-A at 1,956 cm^{-1}, Ni-B at 1,955 cm^{-1} and Ni-SI_r at 1,922 cm^{-1} [25]). The bands in the region from 2,100 to 2,050 cm^{-1} are associated with the CN^- stretching vibrations (two per state). The high frequency absorption band is assigned to the in-phase (symmetric) vibration of the CN^- ligands and the low frequency absorption band is assigned to the out-of-phase (asymmetric) vibration. Those bands corresponding to Ni-A, Ni-B and Ni-SI_r are well resolved (Fig. 3a; Table 1). An additional CO band at 1,964 cm^{-1} was observed in all sample preparations. The intensity of this CO band did not increase in preparations with different pH, whereas the CN^- stretching vibrations that are probably related to such a state (Ni-S_{1964}, EPR-silent) could not be resolved. However, it can be electrochemically reduced and reoxidized. The reoxidized fraction was significantly smaller (approximately 40% of the initial intensity). Additional states in the as-isolated enzyme preparations have also been observed in *Allochromatium* (*A.*) *vinosum* [24], where they were attributed to completely inactive species or states that carry a sulphur-based ligand [24]. This state in the case of *D. vulgaris* is presumably an oxygen-inhibited state, conformationally different from the Ni-SI_r as a result of the purification procedure. From the apparent integrated intensities of these peaks and assuming equal absorption coefficients, we estimated that 80% of the sample contains a mixture of the paramagnetic Ni-A and Ni-B states (approximately 30% Ni-A and 50% Ni-B). The rest of the sample (approximately 20%) contains mostly the Ni-SI_r state and to a lesser extent the Ni-S_{1964} state.

Low temperature FTIR measurements

Figure 3b shows the FTIR spectrum of the aerobically isolated [NiFe] hydrogenase from *D. vulgaris* Miyazaki F at 95 K. The positions of the absorption bands at low temperatures are shifted by 0–5 cm^{-1} in comparison with those obtained at room temperature (297 K; Table 1). This is a general property of the stretching bands observed in infrared and Raman spectroscopies [43] and is related to the restricted vibrational freedom of the oscillators.

Figure 3c shows an FTIR difference spectrum (light-minus-dark). This spectrum shows only the bands of the light-sensitive states (educts, negative absorption bands) and those of the light-induced states (products, positive absorption bands). The negative CO bands observed in the spectrum correspond to Ni-SI_r (1,922 cm^{-1}) and to a new state named Ni-SI_{1961} in this work (denoted by its CO stretching vibration at 1,961 cm^{-1}). As a product we observed only one positive CO band (1,968 cm^{-1}), which was associated with a new light-induced state (named Ni-SL) (Fig. 3c). The infrared spectra show that both Ni-SI_r and Ni-SI_{1961} convert to a light-induced product state (i.e. Ni-SL). However, it is not possible at this point to affirm whether Ni-SI_{1961} is present in the initial dark spectrum (Fig. 3b). The presence of this band and its possible involvement in the photochemical processes observed will be described later in this work. The light sensitivity observed by FTIR spectroscopy in the aerobically isolated sample was also monitored by EPR spectroscopy (X-band, approximately 9.4 GHz). No new EPR signals were observed upon illumination (data not shown). This suggests that the light-induced Ni-SL state is EPR-silent (Ni^{2+}).

Table 1 Stretching vibrations of the CO and CN^- ligands for the different states of the [NiFe] hydrogenase from *Desulfovibrio vulgaris* Miyazaki F measured in this work, at 297 and 95 K

States	IR frequencies							
	$T = 297$ K				$T = 95$ K			
	$\tilde{\nu}_{CO}$ (cm^{-1})	$\tilde{\nu}_{CN\ (asym)}$ (cm^{-1})	$\tilde{\nu}_{CN\ (sym)}$ (cm^{-1})	$\tilde{\nu}_{CO\ (ext)}$ (cm^{-1})	$\tilde{\nu}_{CO}$ (cm^{-1})	$\tilde{\nu}_{CN(asym)}$ (cm^{-1})	$\tilde{\nu}_{CN(sym)}$ (cm^{-1})	$\tilde{\nu}_{CO(ext)}$ (cm^{-1})
Ni-B	1,955	2,081	2,090	–	1,957	2,082	2,092	–
Ni-A	1,956	2,085	2,094	–	1,957	2,087	2,098	–
Ni-SU	1,958	2,089	2,100	–	–	–	–	–
Ni-SI_r	1,922	2,060	2,070	–	1,922	2,061	2,071	–
Ni-SI_a[a]	1,943	2,074	2,086	–	1,946	2,077	2,090	–
Ni-C[a,b]	1,961	2,074	2,085	–	1,963	2,076	2,088	–
Ni-L[b]	Not observed			–	1,911	2,048	2,063	–
N-SL	Not observed			–	1,968	2,076	2,090	–
Ni-SI_{1961}	Not observed			–	1,961	2,067	2,086	–
Ni-SCO	1,941	2,071	2,084	2,056	1,941	2,072	2,086	2,061

[a] The values for Ni-SI_a, Ni-C (T = 297 K) were taken from Reference [25]

[b] The values for Ni-C/Ni-L (T = 95 K) were taken from the work of [47]

In addition, Fig. 3c shows a small negative CO band at 1,957 cm^{-1}, which is associated with the fully oxidized enzyme (i.e. Ni-A, Ni-B), and the corresponding positive CO band (product state) at 1,975 cm^{-1}. This indicates that a small fraction of the oxidized enzyme is also light-sensitive. This effect was not reversible, when irradiation was performed with white light. Therefore, it might be related to a form of photodegradation. Quantification based on the integrated intensity of these peaks shows that this corresponds to 4% (±2%) of the initial amount of oxidized states. Similar light effects at cryogenic temperatures have previously been observed in the cyanobacterial-like uptake hydrogenase from *Acidithiobacillus ferrooxidans* [44].

Figure 3d shows the light-minus-dark difference spectrum after dark adaptation and reillumination of the sample. Since the small effect on the fully oxidized enzyme was not reversible (when illumination was performed with white light),[2] the corresponding bands (educts and products) do not appear in this spectrum. A similar light-minus-dark difference spectrum as for the aerobically isolated enzyme was also obtained for hydrogenase samples partially reduced with H_2 (data not shown), in which the amount of Ni-SI_r was approximately 90%.

Light conversion as a function of the illumination time

The light sensitivity of the Ni-SI_r state is clearly observed in the FTIR spectra, in which this state is shown to convert to the product state Ni-SL (Fig. 3c, d). However, the appearance of Ni-SI_{1961} was unexpected. The question arises as to whether this state was already present in the as-isolated sample or whether it is somehow related to the photochemistry observed. Figure 4a shows the process for the light-induced conversion of Ni-SI_r to Ni-SL. The three-dimensional spectrum was obtained by measuring the light-minus-dark difference spectra at different illumination intervals (from 15 to 300 s) at 75 K. Upon illumination there is a fast conversion from Ni-SI_r to Ni-SI_{1961} and simultaneously, as the illumination time increases, both Ni-SI_r and Ni-SI_{1961} convert to Ni-SL.

Figure 4b shows the light-minus-dark difference spectrum after 15 s of illumination at 75 K. The negative CO peak at 1,922 cm^{-1} corresponds to the dark educt (Ni-SI_r). The two positive CO bands correspond to the light products Ni-SI_{1961} and Ni-SL. The peak at 1,961 cm^{-1} is of higher intensity, clearly showing that Ni-SI_r converts initially to Ni-SI_{1961}. The vibrational frequencies of the conjugate CN^- corresponding to Ni-SI_{1961} (2,086 and 2,067 cm^{-1}) could be identified from this spectrum (Table 1). Figure 4b also shows the light-minus-dark difference spectrum after 300 s of illumination at 75 K, in which only the Ni-SL state is observed as the final light product.

Figure 4c shows the time-dependent forward conversion of the three states; transient rise/decay of Ni-SI_{1961}, formation of Ni-SL and disappearance of Ni-SI_r. These curves were obtained from the apparent integrated intensity of the respective CO bands. The time axis represents illumination time in seconds. The decrease of Ni-SI_{1961} to negative values shows that a small fraction of Ni-SI_r converted to the Ni-SI_{1961} state, already in the absence of an external light source (dark conditions). This partial conversion was

[2] These light effects were reversible when illumination was performed with monochromatic light (laser illumination).

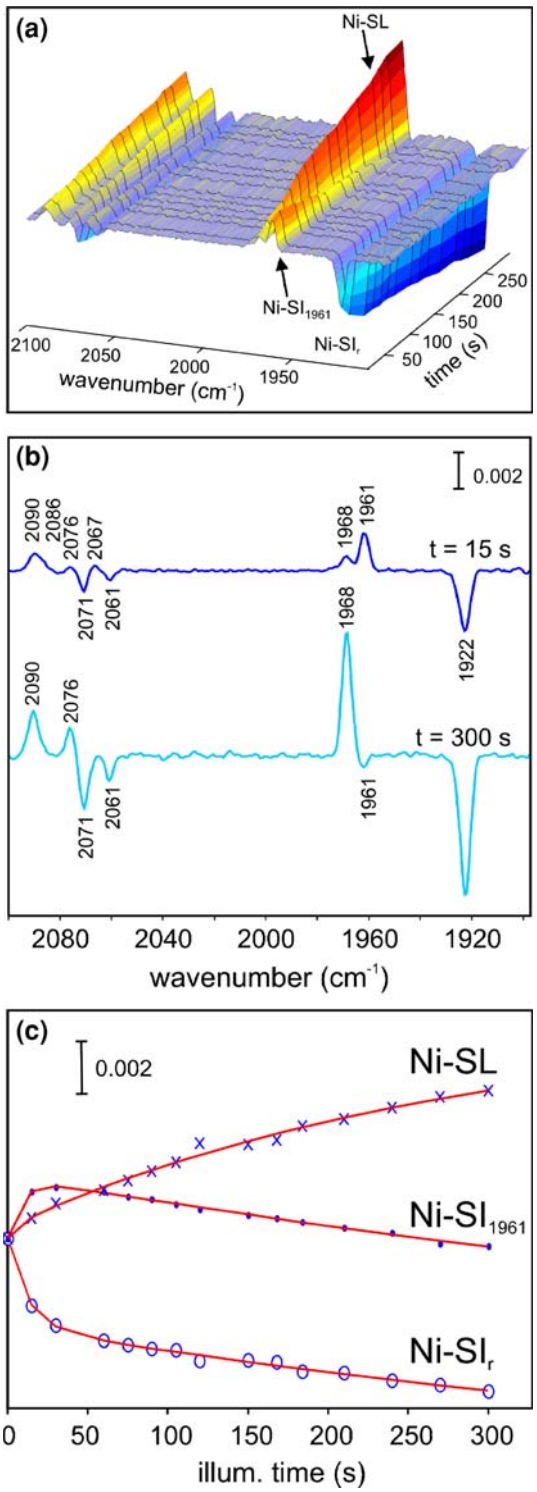

Fig. 4 FTIR light-minus-dark difference spectra recorded at 75 K for different irradiation times. **a** Three-dimensional representation of the photoconversion of the Ni-SI_r state (1,922 cm^{-1}) to Ni-SI_{1961} and Ni-SL using white light as a function of the illumination time. **b** Slices of the three-dimensional representation after 15 and 300 s of illumination illustrating Ni-SI_{1961} as an intermediate in the reaction sequence. **c** Time evolution of the light product and educt states as function of illumination time. The *y*-axes represent the infrared absorbance

due to the spectrometer-integrated He–Ne laser (λ = 633 nm, see "Materials and methods"). The Ni-SI_{1961} state is suggested to be a local minimum in the potential surface of the transition from Ni-SI_r to its final product Ni-SL.

Kinetic measurements and isotope (H/D) exchange effect

Figure 5a depicts the recovery of the absorption bands in the light-minus-dark difference FTIR spectrum at 95 K. Continuous illumination was carried out for 5 min as described in "Materials and methods". The first slice of the three-dimensional spectrum corresponds to $t = 0$, when the light source was switched off (maximum light-minus-dark difference) and the subsequent slices show how the FTIR absorption bands disappear/recover in the dark (Ni-SL, Ni-SI_r and Ni-SI_{1961}). The light-induced effects associated with these states are fully reversible. During back conversion there is no transient increase of the Ni-SI_{1961} state, which indicates that only Ni-SL to Ni-SI_r/Ni-SI_{1961} conversion and vice versa can be observed at temperatures of 80 K and above. The transition from Ni-SL to Ni-SI_r presumably still occurs via the Ni-SI_{1961} state, but under these conditions is too fast to be resolved.

Figure 5b shows the kinetics during dark adaptation of the educt and product states after 5 min of continuous illumination at 95 K. Assuming a single-exponential decay/increase of the signals, we estimated the corresponding rate constants. The Ni-SI_{1961} state recovers 1.5 times faster than the Ni-SI_r state. The kinetics of the disappearance of Ni-SL has values intermediate between those for the recovery kinetics observed for Ni-SI_r and Ni-SI_{1961}. The rate constants exhibited a temperature dependence, which shows that the light-induced processes are associated with an activation energy barrier (E_a).

Figure 5c shows the temperature dependence of the measured rate constants corresponding to the decay of the Ni-SL state in the temperature range between 90 and 110 K. Similar plots were obtained for the Ni-SI_r and Ni-SI_{1961} states (see the electronic supplementary material). The activation energies for Ni-SI_r, Ni-SI_{1961} and Ni-SL were obtained from the linear behaviour of the temperature dependence of all rate constants using the Arrhenius equation (see "Materials and methods"). Similar activation energies were obtained within the error for the Ni-SI_r, Ni-SI_{1961} and Ni-SL states (Table 2).

To study a possible isotope effect on the rate constants, samples were prepared in which the potential third bridging ligand (e.g. OH^-) [4, 5, 24] was exchanged with its deuterated form (OD^-). The activation energies for the isotopically (H/D) exchanged samples were also determined from the Arrhenius dependence of the kinetic rates. The

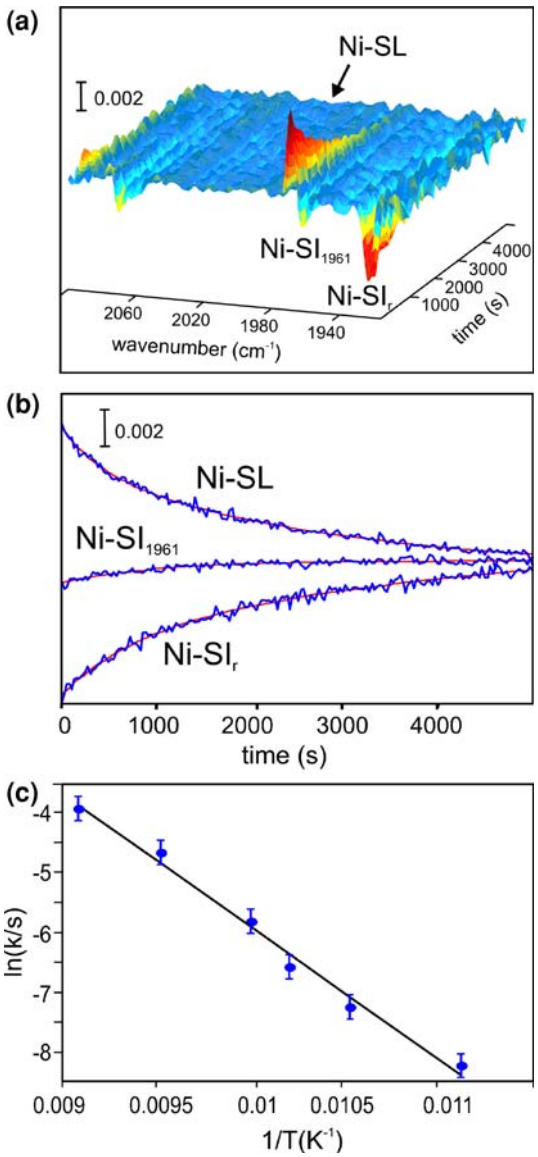

Fig. 5 Time dependence of the recovery of the Ni-SI_r and Ni-SI_{1961} states and the decay of the Ni-SL state at 95 K directly after switching off the light. **a** Three-dimensional representation of the FTIR light-minus-dark difference rapid scan spectrum. **b** Decay kinetics of Ni-SL (1,968 cm^{-1}, $\tau = 1{,}394$ s) and recovery kinetics of Ni-SI_r (1,922 cm^{-1}, $\tau = 2{,}203$ s) and Ni-SI_{1961} (1,961 cm^{-1}, $\tau = 1{,}305$ s). The *y*-axis represents the infrared absorbance. **c** Temperature dependence (in the range between 90 and 110 K) of the decay rate constants for the Ni-SL state (Arrhenius plot)

results showed slightly larger activation energies for the samples containing the deuterated form of this ligand (Table 2 and electronic supplementary material).

Reversible light effects in the presence of CO

In the light-induced process of conversion from Ni-SI_r to Ni-SL, the fate of the oxygen-based bridging ligand is not clear. This ligand is either completely dissociated from the active site or displaced towards nickel, presumably as a consequence of loss of its bond to iron (as reflected by the shift of the infrared frequencies, see "Discussion"). It is known from extensive stopped-flow studies on *A. vinosum* [20, 29, 40] that the oxidized states Ni-A, Ni-B and Ni-SI_r are not CO-sensitive. However, Ni-SI_a and Ni-L are CO-sensitive, allowing the binding of CO to the active site (Fig. 2). This suggests that for CO binding to take place, the bridging ligand must be absent [38]. In the case of complete dissociation of the bridging ligand, dark adaptation of the Ni-SL in the presence of CO would lead to formation of a CO-inhibited state, whereas in the case of its displacement towards nickel this ligand would still block the entrance to the active site, precluding binding of CO. An experiment was thus designed in which the solution of reduced hydrogenase (approximately −300 mV, vs the normal hydrogen electrode), containing mainly the Ni-SI_r and Ni-SI_a states, was saturated with CO.

A high yield of the Ni-SCO state (approximately 80%) was obtained, with the rest of the hydrogenase molecules being in the Ni-SI_r state. Illumination with white light at 40 K simultaneously converted Ni-SCO to Ni-SI_a, as described earlier [26], and Ni-SI_r to Ni-SL. After dark adaptation at higher temperatures no decrease in the intensity of the Ni-SI_r band was observed within error (data not shown). This shows that exogenous CO does not have the affinity to bind to the active site in the Ni-SL state.

Table 2 Activation energies for the recovery of the Ni-SI_r and Ni-SI_{1961} states and for the decay of Ni-SL, obtained from the temperature dependence of the rate constants (see text)

State	Activation energy E_a (kJ mol^{-1})	
	H_2O	D_2O
Ni-SI_r	18.9 ± 1.4	20.3 ± 0.8
Ni-SI_{1961}	17.6 ± 1.5	19.8 ± 1.1
Ni-SL	18.5 ± 0.8	20.6 ± 0.7

Wavelength dependence of the Ni-SI_r light sensitivity

The transition from Ni-SI_r to the Ni-SI_{1961} and Ni-SL states was also studied as a function of the excitation wavelength of the incident light. The results (i.e. the 'action spectrum') at 40 K are depicted in Fig. 6. This action spectrum describes the overall efficiency of the irradiation at a specific wavelength for the photochemical conversion (i.e. percentage) from Ni-SI_r to Ni-SL to occur. Two local maxima, at 490 and 600 nm, were observed, which can be associated with nickel-centred electronic transitions (see "Discussion").

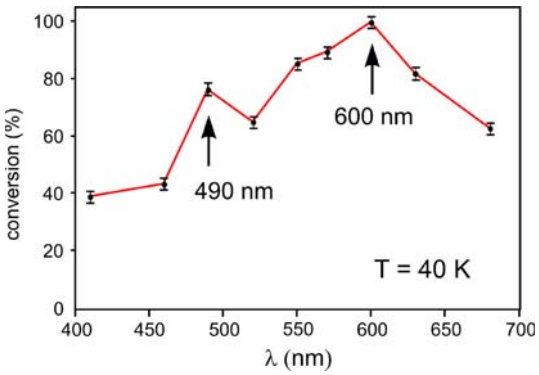

Fig. 6 Photoconversion (%) of the Ni-SI_r state as a function of the irradiation wavelength (λ) at 40 K. The resulting 'action spectrum' shows local maxima at 490 and 600 nm, which can be associated with nickel-centred *d–d* transitions upon light excitation

In addition, the wavelength dependence of the transient appearance of the Ni-SI_{1961} state was studied at 75 K, because at temperatures below 60 K the lifetime of this state was too short for it to be observed as an intermediate in the forward light conversion. Figure 7 shows the development of light-minus-dark difference spectra as a function of the irradiation time at three selected wavelengths. For irradiation at 630 nm (red light), the Ni-SI_r state rapidly converts first to the transient Ni-SI_{1961} state and to a smaller extent to the Ni-SL state. Subsequently, Ni-SI_{1961} is depleted and Ni-SL is populated. The Ni-SI_{1961} state can therefore be considered as a true intermediate state in this reaction. For irradiation at 520 nm (green light), light transition from Ni-SI_r to Ni-SI_{1961} takes place to a much smaller extent, and both states convert to Ni-SL. It can be seen that the CO band corresponding to Ni-SI_{1961} becomes positive but decreases to negative values, as a small fraction of this state is already present under dark conditions. For irradiation at 410 nm (violet light), the spectrum is depicted as a dark-minus-light spectrum to better illustrate the observed processes. Illumination at this wavelength shows that in this transition the Ni-SI_{1961} state could not be resolved as an intermediate of the photoreaction. These results demonstrate that the conversion of Ni-SI_r to Ni-SI_{1961} and subsequently to Ni-SL is strongly temperature and wavelength dependent.

Figure 8 shows that for the Ni-SL state, depending on the excitation wavelength, the stretching modes for the coupled CN^- ligands were shifted, but the frequency of the CO band remained the same. For irradiation with red light (Fig. 8a) the coupled CN^- of Ni-SL are observed at 2,075 and 2,084 cm^{-1}, whereas for irradiation at 410 nm (Fig. 8b) four overlapping CN^- bands are present in the spectra, corresponding to a conjugate CN^- pair with frequencies of 2,075 and 2,084 cm^{-1} and to a second pair of coupled stretching vibrations with frequencies of 2,076 and 2,090 cm^{-1}. If illumination is carried out with white light (halogen lamp; Fig. 8c) only the pair with stretching vibrations at 2,076 and 2,090 cm^{-1} is observed. In all cases, the CO absorption band appears at the same frequency (1,968 cm^{-1}). The invariance of the CO band upon wavelength-dependent illumination precludes a change of the electron density at the iron between these two light-induced forms of Ni-SL, as this would lead to a shift of all three stretching bands (CO and CN^-). The temperature and wavelength dependence of only the CN^- modes therefore indicates a change of the hydrogen bonding with the surrounding amino acids, as described in "Discussion".

Discussion

Light-associated effects on the structure of Ni-SI_r

The silent ready state Ni-SI_r in the [NiFe] hydrogenases represents the link between the fully oxidized and the reduced active enzyme. However, to date the characterization of this state has been rather elusive owing to its inaccessibility to EPR studies and the difficulty to create pure states for other structural investigations [45]. In this work possible structural and electronic properties of Ni-SI_r are discussed on the basis of its light sensitivity.

The infrared spectrum of the aerobically isolated enzyme from *D. vulgaris* consists mainly of bands corresponding to Ni-A, Ni-B and Ni-SI_r. An additional band at 1,964 cm^{-1} was ascribed to a non-identified state (Ni-SI_{1964}), which presumably originates from the enzyme purification procedure. The Ni-A and Ni-B states (Ni^{3+}) exhibited a small light sensitivity (i.e. $4 \pm 2\%$ of their overall intensity; Fig. 3c). This shows that the bridging ligand present in these oxidized states—hydroxide (OH^-) in Ni-B [4, 21] and the proposed hydroperoxide (OOH^-) in Ni-A [13, 14]—is thus quite tightly bound to the Ni^{3+} – Fe^{2+} centre.

On the other hand, upon illumination at cryogenic temperatures ($T \leq 110$ K), Ni-SI_r was shown to convert to a new light-induced state (Ni-SL). Our experiments showed that this light-induced transition involves an intermediate transient state (Ni-SI_{1961}), which was best detected in the temperature range between 60 and 80 K (Fig. 4). EPR spectroscopy showed that Ni-SL is EPR-silent, indicating that the photochemical process is not related to a change in the oxidation state of nickel, which remains divalent (d^8, Ni^{2+}). The light-induced process was fully reversible.

The CO and CN^- stretching bands corresponding to the Ni-SL state are all shifted to higher wavenumbers as

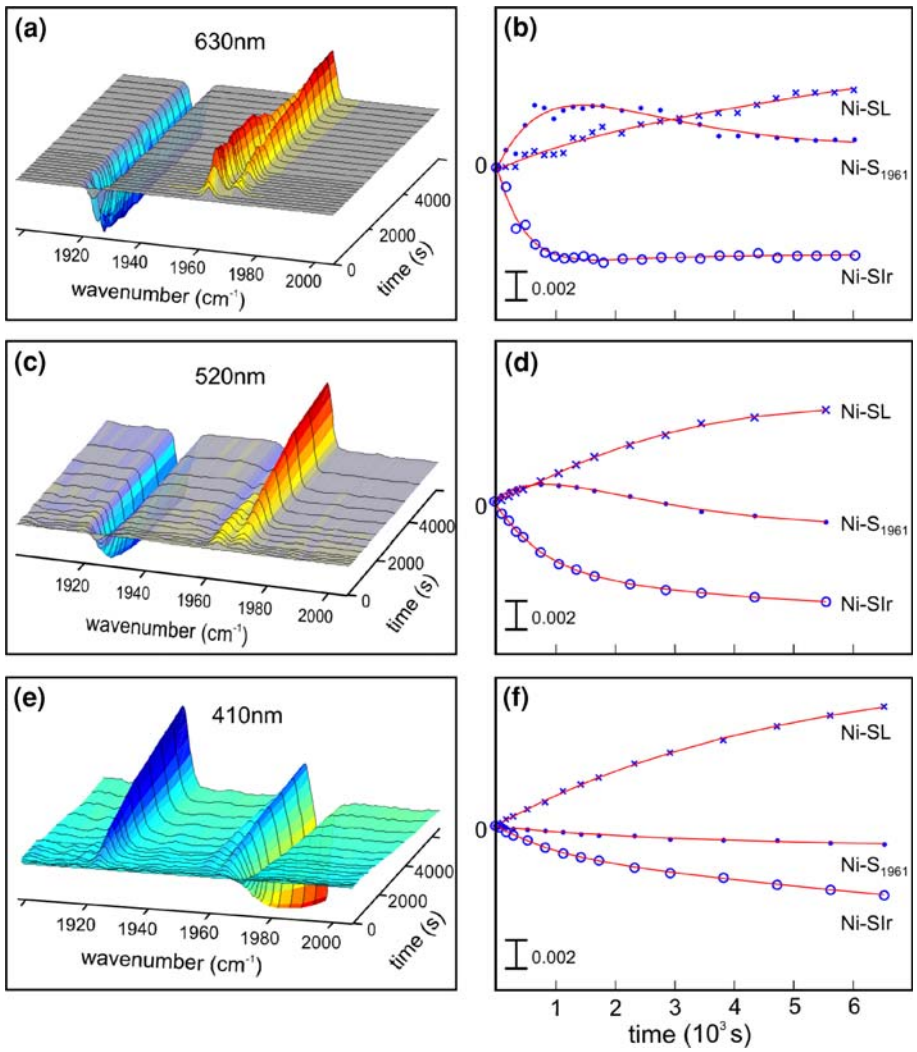

Fig. 7 The forward photoconversion of the Ni-SI_r state to the product states Ni-SI_{1961} and Ni-SL upon irradiation at three selected wavelengths: 630 nm (**a**, **b**), 520 nm (**c**, **d**) and 410 nm (**e**, **f**) at 75 K. The three-dimensional spectra (**a**, **c**, **e**) and plots of the time-dependent kinetics of the appearance/disappearance of the product/educt states are given as function of time (**b**, **d**, **f**). In **e** the three-dimensional spectrum has been inverted (educt/product states as positive/negative signals, respectively), to better visualize the disappearance of the Ni-SI_{1961} state. The *y*-axes represent the infrared absorbance

compared with those of Ni-SI_r (Fig. 3, Table 1). This correlates with a decrease in the electron density at the iron [46] in the light-induced state (Ni-SL). Since all the photochemical properties observed so far in the [NiFe] hydrogenases are associated with dissociation of a non-protein ligand bound to the active site [26, 32, 38], this effect can, in principle, be associated with the removal or displacement of a negatively charged ligand. Since the Fe^{2+} ion is strongly coordinated to σ- and π-ligands (two CN^- and one CO) and to the sulphurs from Cys84 and Cys549 residues (Fig. 1), the most likely candidate is the bridging hydroxide.

A shift towards higher vibrational frequencies has also been observed during the light-induced transition from Ni-SCO to Ni-SI_a [26], which is associated with the dissociation of the extrinsic CO. However, in the photoconversion from Ni-C to Ni-L [46, 47], a shift towards lower wavenumbers was observed. To explain the difference in the direction of the shift, it has been proposed that the dissociation of H^- is followed by the protonation of a coordinating cysteinyl ligand, which would affect the electron density at the Fe^{2+} ion in a different way.

The question arising now is whether the OH^- ligand remains bound to nickel in the Ni-SL state. To answer this question, additional experiments in the presence of CO were performed (see "Results"). The results showed that CO does not bind to the active site in the Ni-SL state. This indicates that the active site remains blocked by the OH^- ligand, thus precluding the binding of CO.

On the basis of these observations and the detected shift in the stretching vibrations, we propose that the light-induced transition from Ni-SI_r to Ni-SL involves opening of the OH^- bridge as depicted in Scheme 1. This displacement of the OH^- ligand is facilitated by the weakening of the OH^- binding to the more electron-rich Ni^{2+} with respect to the Ni^{3+} centre in the fully oxidized enzyme (i.e. Ni-B). The shift in the vibrational bands observed for Ni-SI_{1961} is smaller than that observed for Ni-SL. Thus, the intermediate state might represent a structure in which the OH^- ligand is far less dislocated from the

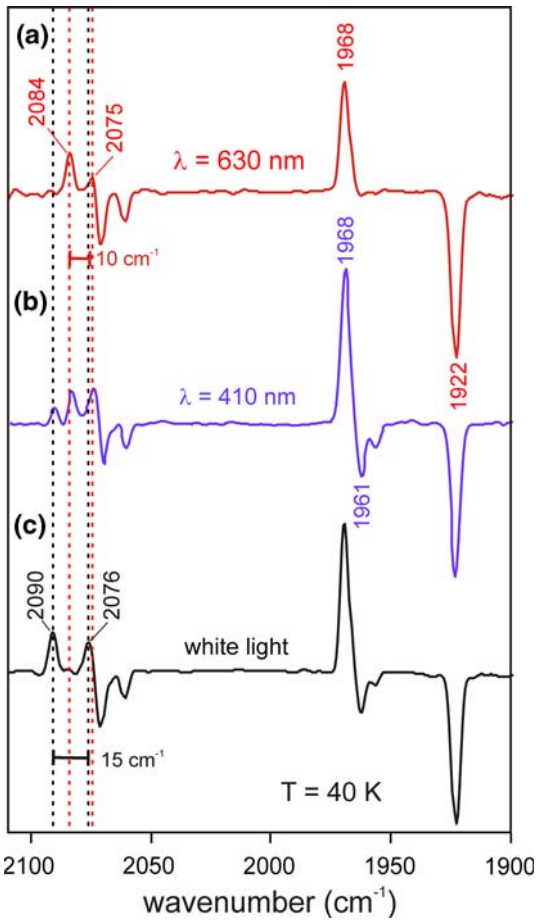

Fig. 8 FTIR light-minus-dark difference spectra for incident irradiation with *a* red light (630 nm), *b* violet light (410 nm) and *c* white light (halogen lamp) at 40 K. Note that depending on the colour of the light, the Ni-SL state shows different pairs of conjugate CN^- stretching vibrations, as indicated with *dashed lines* (see the text)

iron. The absolute intensity of the CN^- bands with respect to the CO band between Ni-SI_{1961} and Ni-SL is different, which might also indicate a change in the hydrogen bonds with the nearby amino acids [48].

The temperature dependence of the kinetic rates corresponding to the back-conversion processes (Ni-SL → Ni-SI_r, Ni-SL → Ni-SI_{1961}) provided the activation energies (E_a), a measure of the energy required to overcome the barrier for the transition from the photoproduct (Ni-SL) to the initial state(s). Even though the recovery rates corresponding to Ni-SI_r and Ni-SI_{1961} are different (Fig. 5b), the activation energies are very similar (Table 2). Furthermore, the (H/D) isotope effect on the recovery kinetic rates was studied (Table 2). The magnitude of the isotope effect in our experiments (kinetic isotope effect of 0.6–1.4, see the electronic supplementary material) was too small to be related to the dissociation of a single hydron species [49],[3] as observed for the Ni-C to Ni-L transition [47]. This result therefore suggests that the light-induced effect is not related to a (de)protonation of a coordinating cysteine [30] or a release of a hydron located in the active site [50]. Thus, the (H/D) isotope effect observed in this work can be better explained considering the dislocation of an oxygen-based species [5, 14, 51] that has the potential to be deuterated (e.g. OH^-).

The small increase in mass introduced by the isotope labelling (e.g. OD^-) is expected to affect slightly the values of the kinetic rates. This is in agreement with our results, supports the proposed reaction shown in Scheme 1 and further rules out processes involving a (de)protonation of a coordinating cysteine [30] or the release of a hydron located in the active site [50].

The activation barrier for the transition of Ni-SL to Ni-SI_r and Ni-SL to Ni-SI_{1961} was found to be 18–19 kJ mol^{-1}. Such a value lies well within the range of energies corresponding to related hydrogen bonds (15–40 kJ mol^{-1}) [52]. This would mean that back conversion from Ni-SL to the Ni-SI_r/Ni-SI_{1961} states could involve the breaking of a hydrogen bond to surrounding amino acids. From the crystal structure of the Ni-B state it can be deduced that the OH^- ligand at the nickel might be in a favourable position to form a hydrogen bond to Arg479 (see below).

Wavelength dependence of the Ni-SI_r photoconversion

It was found that light excitation of Ni-SI_r is described by a broad absorption in the visible region between 410 and 680 nm (Fig. 6). In this 'action spectrum' two local maxima were observed, at 490 and 600 nm. Optical studies on Ni^{2+} complexes with sulphur-based ligands [53, 54] showed bands in MCD spectra close to these values, which were associated with *d–d* transitions of the Ni d^8 ion. It can thus be assumed that in the case of Ni-SI_r the action spectrum shows that the photochemical process is associated with electronic excited states of the nickel ion. Although Ni-L-edge X-ray absorption spectroscopy cannot clearly discern whether the nickel ion in Ni-SI_r is in a low-spin ($S = 0$) or a high-spin ($S = 1$) configuration [36], theoretical data [37] indicate a low-spin Ni^{2+}. The light-induced electronic transitions (Fig. 6) could involve a change in the spin state of nickel from a low-spin (d^8, $S = 0$) to a high-spin (d^8, $S = 1$) configuration as a result of the redistribution of the electronic charge in the *d* orbitals of the metal. Such light-induced spin crossover transitions have been shown to involve a ligand rearrangement [55]. A change from low-spin to high-spin could in turn trigger a structural change of the ligand sphere, effectively leading to the observed opening of the bridge of the NiFe centre.

[3] In such a case the kinetic isotope effect should be between 5 and 7 [49].

Scheme 1 Light-induced transition from the Ni-SI_r state to the Ni-SL state involving opening of the hydroxide bridge

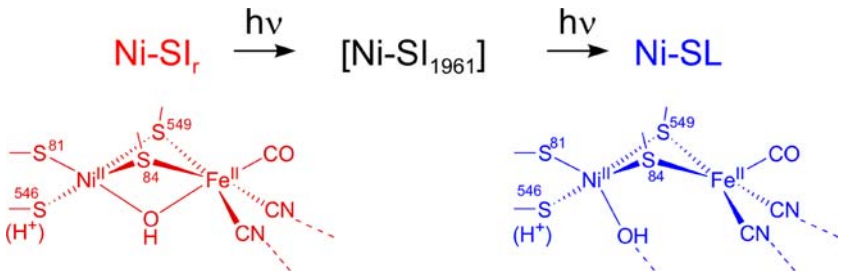

At 40 K and at all excitation wavelengths, Ni-SI_{1961} was not observed as an intermediate in the forward transition of Ni-SI_r to Ni-SL. At higher temperatures, however (e.g. in the range $60\ K < T < 80\ K$) the wavelength-dependent forward photoconversion of Ni-SI_r involved the Ni-SI_{1961} state as a detectable intermediate (Ni-SI_r → Ni-SI_{1961} → Ni-SL) (Fig. 7). The amount of the light-induced Ni-SI_{1961} species depended greatly on the excitation wavelength, being maximal in the red (above 600 nm). However, since the optical transitions of the Ni^{2+}–Fe^{2+} site are not known, it is difficult at present to elucidate a mechanism for the light-triggered evolution of the different states observed in our experiments.

Hydrogen-bonding network in the active-site surroundings

The putative hydrogen bonds between the active centre of the [NiFe] hydrogenase from *D. vulgaris* Miyazaki F and the surrounding amino acids are shown in Fig. 9. The formation of a hydrogen bond between the sulphur of the bridging Cys549 and His88 is well established and has been studied for different states [56–58]. In addition, each of the CN^- ligands at the iron can potentially form up to two hydrogen bonds, as indicated in Fig. 9, whereas the CO ligand is surrounded by more hydrophobic residues and is thus not hydrogen-bonded. It is well known that the environment of such iron ligands greatly affects the redox properties of the central metal [59, 60].

Among the amino acids in the surroundings of the active site, an arginine residue (Arg479) is located very close to the bridging OH^- ligand (Fig. 9). This arginine is highly conserved among the various hydrogenases and is believed to be protonated and positively charged [61]. It is hydrogen-bonded to one of the CN^- ligands and to two negatively charged aspartates (Asp123, Asp544). The light-induced transition from Ni-SI_r to Ni-SL is proposed to involve a displacement of the OH^- ligand to a position closer to nickel (Scheme 1). Since Arg479 is considered to be protonated ($pK_a \sim 12$), this ligand rearrangement would result in a hydrogen bond between the oxygen of the OH^- and the NH of Arg479 (see Fig. 9), with an O–N distance in the range 3.0–3.4 Å. It can be speculated that the intermediate Ni-SI_{1961} in the reaction sequence represents a pathway species with an opened OH^- bridge that has no—or weaker—hydrogen-bond interactions with the surroundings compared with the final Ni-SL state.

In the same figure the putative hydrogen bonds between the CN^- ligands and the amino acid residues Arg479 and Ser502 as well as with the backbone NH of the two prolines[4] are shown. The vibrational frequencies of these ligands depend, therefore, not only on the electron density at the iron but also on the strength of the hydrogen-bonding network [62]. In our experiments the stretching vibrations of the CN^- in Ni-SL were observed to be affected by the wavelength of the exciting light (Fig. 8). On the other hand, the respective $\tilde{\nu}_{CO}$ were not sensitive to the colour of the monochromatic irradiation. Since the CN^- ligands—but not the CO—are hydrogen-bonded to surrounding amino acids, it can be assumed that a change in the hydrogen-bonding network is responsible for this observation. In support of our experiments, a shift in the infrared frequencies only of the CN^- was observed in a study where the serine residue (Ser502 in *D. vulgaris*, Ser499 in *D. fructosovorans*) was mutated to an alanine [48], which is incapable of forming a hydrogen bond.

Figure 8a shows that at 40 K illumination with red light shifts the CN^- bands to lower frequencies compared with illumination with white light (Fig. 8c). Such a shift to lower values indicates a weakening of the hydrogen-bonding [62–64] interactions of these ligands with the surrounding amino acid residues. Illumination with violet light (410 nm; Fig. 8b), on the other hand, resulted in the simultaneous appearance of two pairs of vibrationally coupled CN^-. This observation is important as it shows that transition from one form of Ni-SL (red-light-induced spectrum) to the second form (white-light-induced spectrum) is characterized by distinct electronic levels. In coordination chemistry there are examples of iron compounds, ligated by cyanides and nitrosyls, where light-induced isomers of the diatomic ligands can be observed at

[4] Hydrogen bonds with the backbone of Pro478 and Pro501 are considered less likely as mutation experiments have shown that substitution of Pro478 with alanine had no effect on the infrared spectra [49].

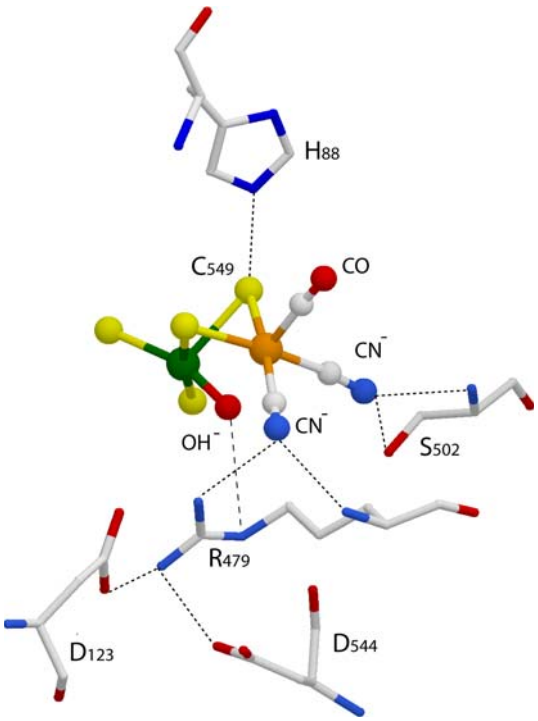

Fig. 9 Proposed structure of the active site of the [NiFe] hydrogenase from *D. vulgaris* Miyazaki F in the Ni-SL state (based on the structure of Ni-B; Protein Data Bank entry 1WUJ). The amino acid residues His88, Arg479 and Ser502 and part (backbone) of Pro480 and Pro478 are shown. The putative hydrogen bonds to the direct ligands of the NiFe complex are represented with *dashed lines*. Note that the hydroxide bridge, present in Ni-SI_r, has been opened in this structure and the OH^- ligand at the nickel is hydrogen-bonded to Arg479

low temperatures. In such light-induced 'linkage isomers' (metastable states) the metal is coordinated (e.g. in nitrosyls) by the oxygen instead of the nitrogen [65, 66]. It might be speculated that in the case of hydrogenase, an Fe–N–C linkage could be realised [67, 68] upon increasing the irradiation wavelength and decreasing the temperature ($T \leq 40$ K). This would result in the loss of the hydrogen bond(s) to the amino acid residues and the concomitant shift of the CN^- vibrations towards lower frequencies [48], as observed in our experiments. Such a situation, however, is purely hypothetical as it is not known whether it is possible for it to occur in a protein environment.

In addition, the CN^- vibrations shift in the same direction, but the magnitudes and intensities are different (Fig. 8). This indicates a change in the coupling between the CN^- oscillators, which, however, remain conjugated. From these results and the invariance of the CO frequency band between these two Ni-SL forms, it becomes evident that changing the irradiation wavelength affects only the CN^- stretching vibrations, i.e. the hydrogen-bonding interactions, and not the electron density at the iron. The existence of the surrounding hydrogen-bonding network and/or electrostatic interactions is therefore important for stabilizing and 'tuning' the active-site conformation.

Summary and conclusions

The FTIR data presented in this work provided an effective means to characterize the active site of Ni-SI_r. Conformational changes upon exposing Ni-SI_r to light ($T \leq 110$ K) are observed by the appearance of new product states. These changes consist of a structural rearrangement of the negatively charged hydroxide ligand (OH^-), proposed to ligate the active site. The light-induced reorientation of the oxygen-based species involves a transient intermediate (Ni-SI_{1961}) prior to reaching Ni-SL as the final steady state. Such a displacement is facilitated by the weakening of the OH^- binding to the more electron rich Ni^{2+}, in contrast to the more oxidized Ni^{3+} species. In support of this statement, only a minor light sensitivity was observed for the Ni-A and Ni-B states. On the basis of the X-ray diffraction data of the Ni-B state, we propose that the position of the hydroxide in Ni-SL can be stabilized by the formation of a hydrogen bond to Arg479. From this position, the oxygen-based ligand is still blocking access to the active site, as presumably it remains coordinated to the nickel ion. This was presented by the inability of extrinsic CO to bind to nickel. Therefore, upon illumination the oxygenic ligand is spatially displaced rather than fully dissociated. Wavelength-dependent irradiation indeed showed nickel-centred electronic transitions, which could involve a light-induced spin crossover from a low-spin Ni^{2+} ($S = 0$) to a high-spin Ni^{2+} ($S = 1$). However, to uniquely assign these transitions, further MCD measurements are needed. The hydrogen-bonding and/or electrostatic interactions of the active site with the neighbouring amino acid residues were shown to be modulated by the colour of the monochromatic light. Spectral changes associated only with the CN^- and not with the CO preclude a change in the iron electron density, as the CO has been shown to be approximately 2–3 times more sensitive to electronic changes than the cyanides [64]. We propose that the reason for this 'perturbation' of the hydrogen-bonding network around the CN^- ligands as revealed in our experiments could be caused by a light-induced isomerization. To prove this assumption further experiments including labelling of the intrinsic CN with ^{13}C and ^{15}N are required.

In the reactivation scheme, the oxygenic species has to be released from the active centre for the enzyme to be functional. From the results of the present study, we conclude that an oxygen-based ligand (i.e. OH^-) is still bound to the active site, which hinders the enzymatic activity. In Ni-SI_r the binding strength of this species is found to be attenuated compared with that in Ni-A and Ni-B. Illumination of Ni-SI_r with light at $T \leq 110$ K was adequate to

overcome the activation energy barrier for the displacement of this ligand.

Acknowledgments Kim Bagley, Zhujun Chen and Shan Huang (Buffalo State University, New York) are gratefully acknowledged for sharing their previous observations on the light sensitivity related to the *D. vulgaris* and *A. vinosum* hydrogenases. Stimulating remarks and discussions with Simon Albracht (University of Amsterdam), Karl Wieghardt and Helmut Görner (Max-Planck-Institut für Bioanorganische Chemie) are also gratefully acknowledged. The authors are also thankful to Rita Gröver, Birgit Deckers, Patricia Malkowski, Gudrun Klihm, Frank Reikowski and Christoph Laurich for technical support and assistance. This work was supported by the Max Planck Society, by the EU/Energy Network project SOLAR-H2 (FP7 contract 212508) and BMFT (Bio H2).

References

1. Vignais PM, Billoud B (2007) Chem Rev 107:4206–4272
2. Albracht SPJ (1994) Biochim Biophys Acta 1188:167–204
3. Volbeda A, Charon MH, Piras C, Hatchikian EC, Frey M, FontecillaCamps JC (1995) Nature 373:580–587
4. Lubitz W, Reijerse E, van Gastel M (2007) Chem Rev 107:4331–4365
5. Fontecilla-Camps JC, Volbeda A, Cavazza C, Nicolet Y (2007) Chem Rev 107:4273–4303
6. Nicolet Y, Lemon BJ, Fontecilla-Camps JC, Peters JW (2000) Trends Biochem Sci 25:138–143
7. Silakov A, Reijerse EJ, Albracht SPJ, Hatchikian EC, Lubitz W (2007) J Am Chem Soc 129:11447–11458
8. Shima S, Pilak O, Vogt S, Schick M, Stagni MS, Meyer-Klaucke W, Warkentin E, Thauer RK, Ermler U (2008) Science 321:572–575
9. Higuchi Y, Yagi T, Yasuoka N (1997) Structure 5:1671–1680
10. Pierik AJ, Roseboom W, Happe RP, Bagley KA, Albracht SPJ (1999) J Biol Chem 274:3331–3337
11. Higuchi Y, Ogata H, Miki K, Yasuoka N, Yagi T (1999) Structure 7:549–556
12. Lamle SE, Albracht SPJ, Armstrong FA (2004) J Am Chem Soc 126:14899–14909
13. Volbeda A, Martin L, Cavazza C, Matho M, Faber BW, Roseboom W, Albracht SPJ, Garcin E, Rousset M, Fontecilla-Camps JC (2005) J Biol Inorg Chem 10:239–249
14. Ogata H, Hirota S, Nakahara A, Komori H, Shibata N, Kato T, Kano K, Higuchi Y (2005) Structure 13:1635–1642
15. van der Zwaan JW, Albracht SPJ, Fontijn RD, Roelofs YBM (1986) Biochim Biophys Acta 872:208–215
16. Lamle SE, Albracht SPJ, Armstrong FA (2005) J Am Chem Soc 127:6595–6604
17. Zorin NA, Dimon B, Gagnon J, Gaillard J, Carrier P, Vignais PM (1996) Eur J Biochem 241:675–681
18. Vincent KA, Belsey NA, Lubitz W, Armstrong FA (2006) J Am Chem Soc 128:7448–7449
19. Fernandez VM, Hatchikian EC, Patil DS, Cammack R (1986) Biochim Biophys Acta 883:145–154
20. Kurkin S, George SJ, Thorneley RNF, Albracht SPJ (2004) Biochemistry 43:6820–6831
21. van Gastel M, Matthias M, Brecht M, Schröder O, Lendzian F, Bittl R, Ogata H, Higuchi Y, Lubitz W (2006) J Biol Inorg Chem 11:41–51
22. Volbeda A, Fontecilla-Camps JC (2005) Coord Chem Rev 249:1609–1619
23. De Lacey AL, Hatchikian EC, Volbeda A, Frey M, Fontecilla-Camps JC, Fernandez VM (1997) J Am Chem Soc 119:7181–7189
24. Bleijlevens B, van Broekhuizen FA, de Lacey AL, Roseboom W, Fernandez VM, Albracht SPJ (2004) J Biol Inorg Chem 9:743–752
25. Fichtner C, Laurich C, Bothe E, Lubitz W (2006) Biochemistry 45:9706–9716
26. Bagley KA, Vangarderen CJ, Chen M, Duin EC, Albracht SPJ, Woodruff WH (1994) Biochemistry 33:9229–9236
27. Dole F, Fournel A, Magro V, Hatchikian EC, Bertrand P, Guigliarelli B (1997) Biochemistry 36:7847–7854
28. Jones AK, Lamle SE, Pershad HR, Vincent KA, Albracht SPJ, Armstrong FA (2003) J Am Chem Soc 125:8505–8514
29. George SJ, Kurkin S, Thorneley RNF, Albracht SPJ (2004) Biochemistry 43:6808–6819
30. Bruschi M, Zampella G, Fantucci P, De Gioia L (2005) Coord Chem Rev 249:1620–1640
31. De Lacey AL, Fernandez VM, Rousset M, Cammack R (2007) Chem Rev 107:4304–4330
32. Brecht M, van Gastel M, Buhrke T, Friedrich B, Lubitz W (2003) J Am Chem Soc 125:13075–13083
33. Foerster S, van Gastel M, Brecht M, Lubitz W (2005) J Biol Inorg Chem 10:51–62
34. van der Zwaan JW, Albracht SPJ, Fontijn RD, Slater EC (1985) FEBS Lett 179:271–277
35. Wang HX, Ralston CY, Patil DS, Jones RM, Gu W, Verhagen M, Adams M, Ge P, Riordan C, Marganian CA, Mascharak P, Kovacs J, Miller CG, Collins TJ, Brooker S, Croucher PD, Wang K, Stiefel EI, Cramer SP (2000) J Am Chem Soc 122:10544–10552
36. Wang H, Patil DS, Ralston CY, Bryant C, Cramer SP (2001) J Electr Spectrosc Rel Phenom 114:865–871
37. Jayapal P, Robinson D, Sundararajan M, Hillier IH, McDouall JJW (2008) Phys Chem Chem Phys 10:1734–1738
38. Ogata H, Mizoguchi Y, Mizuno N, Miki K, Adachi S, Yasuoka N, Yagi T, Yamauchi O, Hirota S, Higuchi Y (2002) J Am Chem Soc 124:11628–11635
39. De Lacey AL, Stadler C, Fernandez VM, Hatchikian EC, Fan HJ, Li S, Hall MB (2002) J Biol Inorg Chem 7:318–326
40. Happe RP, Roseboom W, Albracht SPJ (1999) Eur J Biochem 259:602–608
41. Yagi T, Kimura K, Daidoji H, Sakai F, Tamura S, Inokuchi H (1976) J Biochem 79:661–671
42. Atkins P, De Paula J (2006) Atkins' physical chemistry, 8th edn. Oxford University Press, New York
43. Nyquist RA (1986) Appl Spectrosc 40:79–85
44. Schröder O, Bleijlevens B, de Jongh TE, Chen ZJ, Li TS, Fischer J, Förster J, Friedrich CG, Bagley KA, Albracht SPJ, Lubitz W (2007) J Biol Inorg Chem 12:212–233
45. Davidson G, Choudhury SB, Gu ZJ, Bose K, Roseboom W, Albracht SPJ, Maroney MJ (2000) Biochemistry 39:7468–7479
46. Bagley KA, Duin EC, Roseboom W, Albracht SPJ, Woodruff WH (1995) Biochemistry 34:5527–5535
47. Kellers P, Pandelia ME, Currell LJ, Görner H, Lubitz W (2009) Phys Chem Chem Phys (submitted)
48. De Lacey AL, Fernandez VM, Rousset M, Cavazza C, Hatchikian CE (2003) J Biol Inorg Chem 8:129–134
49. De Lacey AL, Pardo A, Fernandez VM, Dementin S, Adryanczyk-Perrier G, Hatchikian EC, Rousset M (2004) J Biol Inorg Chem 9:636–642
50. Fan HJ, Hall MB (2001) J Biol Inorg Chem 6:467–473
51. Armstrong FA (2004) Curr Opin Chem Biol 8:133–140
52. Jeffrey GA (1997) An introduction to hydrogen bonding. Oxford University Press, New York
53. Kozlowski H, Reverend BD-L, Ficheux D, Loucheux C, Sovago I (1987) J Inorg Biochem 29:187–197

54. Kulon K, Wozniak D, Wegner K, Grzonka Z, Kozlowski H (2007) J Inorg Biochem 101:1699–1706
55. Khalil M, Marcus MA, Smeigh AL, McCusker JK, Chong HH, Schoenlein RW (2006) J Phys Chem A 110:38–44
56. Chapman A, Cammack R, Hatchikian CE, McCracken J, Peisach J (1988) FEBS Lett 242:134–138
57. Buhrke T, Lenz O, Porthun A, Friedrich B (2004) Mol Microbiol 51:1677–1689
58. Agrawal AG, van Gastel M, Gärtner W, Lubitz W (2006) J Phys Chem B 110:8142–8150
59. Pereira MM, Teixeira M (2004) Biochim Biophys Acta 1655:340–346
60. Pylypenko O, Schlichting I (2004) Annu Rev Biochem 73:991–1018
61. Lill SO, Siegbahn PE (2009) Biochemistry 48:1056–1066
62. Darensbourg MY, Lyon EJ, Smee JJ (2000) Coord Chem Rev 206:533–561
63. Liaw WF, Chiang CY, Lee GH, Peng SM, Lai CH, Darensbourg MY (2000) Inorg Chem 39:480–484
64. Lai CH, Lee WZ, Miller ML, Reibenspies JH, Darensbourg DJ, Darensbourg MY (1998) J Am Chem Soc 120:10103–10114
65. Carducci MD, Pressprich MR, Coppens P (1997) J Am Chem Soc 119:2669–2678
66. Morioka Y, Takeda S, Tomizawa H, Miki E (1998) Chem Phys Lett 292:625–630
67. Braunstein P, Herberich GE, Neuschtz M, Schmidt MU (1999) J Organometal Chem 580:66–71
68. Woike T, Dahaoui S, Schaniel D, Ponou S, Hansen NK, Petrick V (2004) Zeitschrift für Kristallographie 219:558–566